Isospin and deformation studies in the odd-odd $N = Z$ nucleus ^{54}Co

D. Rudolph,[1] L.-L. Andersson,[1,*] R. Bengtsson,[2] J. Ekman,[1,†] O. Erten,[1,‡] C. Fahlander,[1] E. K. Johansson,[1] I. Ragnarsson,[2] C. Andreoiu,[1,§] M. A. Bentley,[3,‖] M. P. Carpenter,[4] R. J. Charity,[5] R. M. Clark,[6] P. Fallon,[6] A. O. Macchiavelli,[6] W. Reviol,[5] D. G. Sarantites,[5] D. Seweryniak,[4] C. E. Svensson,[6,¶] and S. J. Williams[3,**]

[1]*Department of Physics, Lund University, S-22100 Lund, Sweden*

[2]*Department of Mathematical Physics, LTH, Lund University, S-22100 Lund, Sweden*

[3]*School of Chemistry and Physics, Keele University, Keele, Staffordshire, ST5 5BG United Kingdom*

[4]*Physics Division, Argonne National Laboratory, Argonne, Illinois 60439, USA*

[5]*Chemistry Department, Washington University, St. Louis, Missouri 63130, USA*

[6]*Nuclear Science Division, Lawrence Berkeley National Laboratory, Berkeley, California 94720, USA*

(Received 6 September 2010; published 15 November 2010)

High-spin states in the odd-odd $N = Z$ nucleus ^{54}Co have been investigated by the fusion-evaporation reaction ^{28}Si(^{32}S,$1\alpha 1p1n$)^{54}Co. Gamma-ray information gathered with the Ge detector array Gammasphere was correlated with evaporated particles detected in the charged particle detector system Microball and a 1π neutron detector array. A significantly extended excitation scheme of ^{54}Co is presented, which includes a candidate for the isospin $T = 1$, 6^+ state of the $1f_{7/2}^{-2}$ multiplet. The results are compared to large-scale shell-model calculations in the fp shell. Effective interactions with and without isospin-breaking terms have been used to probe isospin symmetry and isospin mixing. A quest for deformed high-spin rotational cascades proved negative. This feature is discussed by means of cranking calculations.

DOI: 10.1103/PhysRevC.82.054309 PACS number(s): 21.60.Cs, 23.20.Lv, 27.40.+z

I. INTRODUCTION

The spectroscopy of doubly magic nuclei and isotopes in their immediate surroundings provides viable benchmarks of effective nucleon-nucleon interactions. Clearly, these interactions have to be able to describe such core nuclei, before explorations into the extremes of isospin become meaningful.

The regime around the doubly magic $N = Z = 28$ nucleus ^{56}Ni is of specific interest. First, the gap at particle number 28 is classically the first one being generated by spin-orbit splitting [1,2], i.e., a prime ground for studying the strength and origin of the spin-orbit force in finite nuclei. Second, mass $A \sim 60$ nuclei are both sufficiently heavy for profound mean-field studies *and* sufficiently light for modern large-scale fp shell-model calculations [3,4], which are known to provide high-quality wave functions. In addition, the latter allows for detailed investigations of, for example, isospin-breaking terms in the interactions, making $N \sim Z$ fp-shell nuclei suitable candidates for such "mirror studies" [5]. Another facet is the weakness of the magicity at $N = Z = 28$. This is established both experimentally [6] and theoretically (see, e.g., Refs. [7–10]): Correlations between nucleons in the $1f_{7/2}$ orbital below and the $2p_{3/2}$ orbital above the gap allow for collective $E2$ excitations, which give rise to both enhanced $B(E2, 2^+ \rightarrow 0^+)$ rates in light even-even nickel isotopes [6,11,12] or relatively low-lying four-particle four-hole (4p-4h) states [13] creating another, this time deformed $N = Z = 28$ shell gap at distinct prolate shapes [3]. Many of these nuclear structure issues also reappear in the more exotic region around ^{100}Sn, one major oscillator shell higher.

In the present article, the odd-odd $N = Z = 27$ nucleus ^{54}Co is revisited, thus providing refined knowledge on the proton-hole-neutron-hole channel with respect to ^{56}Ni, and in particular on the $A = 54$, $1f_{7/2}{}^{-2}$ multiplet. Here, the isospin $T = 1$, 6^+ state in ^{54}Co remains to be identified (likewise in $N = Z = 21$ ^{42}Sc, see, e.g., Ref. [14] and references therein). The location of this state is considered decisive for detailed studies on nuclear isospin nonconserving parts of isotensor character [15], which requires complete knowledge of isospin triplets such as ^{54}Fe, ^{54}Co, and ^{54}Ni [16–18]. More recently, γ-ray spectroscopic investigations of low- to medium-spin states have been presented, which established a rather comprehensive decay scheme on top of the 0^+ ground state [19] and a limited amount of excited states decaying into the β-decaying 7^+ isomer positioned at 197 keV excitation energy [20]. None of these studies provides a comprehensive interpretation of the observed near-spherical states with contemporary fp shell interactions. Moreover, only rather simple shell-model calculations have been used in a follow-up Letter of Ref. [19], where the authors derive the amount of isospin mixing in two energetically close, predominantly $T = 0$ and $T = 1$, 4^+ states based on $E2/M1$ mixing ratios of their γ decays into lower-lying $T = 0$, 3^+, and 5^+ states [21].

*Present address: Department of Physics, University of Liverpool, Liverpool, L69 7ZE United Kingdom.

†Present address: Malmö högskola, S-20506 Malmö, Sweden.

‡Present address: Department of Physics, Ohio State University, Columbus, Ohio, USA 43210.

§Present address: Chemistry Department, Simon Fraser University, Burnaby, British Columbia V5A 1S6, Canada.

‖Present address: Department of Physics, University of York, Heslington, York, YO10 5DD United Kingdom.

¶Present address: Department of Physics, University of Guelph, Guelph, Ontario N1G 2W1, Canada.

**Present address: TRIUMF, Vancouver, British Columbia V6T 2A3, Canada.

Well- or superdeformed rotational bands have been observed in the vicinity of ^{56}Ni, centered around the $N = Z = 30$ doubly magic superdeformed core ^{60}Zn [22]. Thereby, the most strongly deformed systems are typically built on the 4p-4h excitation across the spherical $N = Z = 28$ gap, and a given number of nucleons in the prolate shape-driving $\mathcal{N} = 4$, $1g_{9/2}$ intruder orbital. This scheme is found valid in, for example, $N = Z = 30$ ^{60}Zn [22], $N = Z = 29$ ^{58}Cu [23], and an excited band in $N = Z = 28$ ^{56}Ni itself [3]. The question remains whether similarly energetically favored configurations exist in lighter nuclei. Naturally, $N = Z = 27$ ^{54}Co is a very well-suited candidate for such a search, which could add information on the spin-orbit strength in the fp shell, as well as the relative location of deformed $1g_{9/2}$ Nilsson levels and thus the spherical $1g_{9/2}$ orbital with respect to fp-shell orbitals.

II. EXPERIMENTAL DETAILS

The present work is based on data from two experiments, which were performed under nearly identical conditions. They are described in more detail in, for example, Refs. [24–26]. Both experiments used the fusion-evaporation reaction ^{32}S+^{28}Si at 130 MeV beam energy. The sulfur beam particles impinged on enriched 0.5 mg/cm^2 ^{28}Si targets supported with approximately 1 mg/cm^2 Ta or Au foils, which faced the beam. The effective beam energy at midtarget was thus only about 122 MeV. The γ rays were detected in the Gammasphere array [27], which for both experiments comprised 78 Ge-detector modules. The Heavimet collimators in front of the Compton suppression shields were removed to allow for the measurement of the total γ-ray energy and fold for each event, which provides additional reaction channel selectivity [28]. The 4π CsI(Tl)-array Microball [29] aimed at the detection of evaporated light charged particles. The Neutron Shell [30], consisting of 30 liquid-scintillator detectors, replaced the five most forward rings of Gammasphere to enable the detection of evaporated neutrons. This type of setup is particularly efficient for the study of weak reaction channels at and beyond the $N = Z$ line. The event trigger required either three or more Ge detectors and one prediscriminated neutron in coincidence or four or more Ge detectors in coincidence.

The fusion-evaporation reaction leads to the odd-odd $N = Z = 27$ nucleus ^{54}Co following the evaporation of one α particle, one proton, and one neutron from the compound nucleus ^{60}Zn. The relative experimental fusion-evaporation cross section of ^{54}Co can be estimated to $\sim$0.2% from yields of ground-state transitions of different residual nuclei. With a total fusion cross section of $\sigma \sim 1.0$ b at a 122-MeV beam energy midtarget, this corresponds to a production cross section of ^{54}Co residues of approximately 2 mb.

The average beam energy of 122 MeV converts into a center-of-mass energy of about 64 MeV of the compound nucleus ^{60}Zn. Considering the differences in binding energies of ^{60}Zn and the residue of interest, ^{54}Co, roughly 40 MeV are available for the kinetic energies of the evaporated particles as well as statistical and discrete γ radiation. Entry states of the compound system are expected to carry average angular momenta of 30–35 $\hbar$ [31]. For the discussion in Sec. V it is important to note that these numbers are almost identical to the reaction ^{28}Si(^{36}Ar,$1\alpha 1p1n$)^{58}Cu at about a 135-MeV effective beam energy. Following that reaction, a very pronounced rotational band in ^{58}Cu was observed, reaching $I^\pi = (23^+)$ at an excitation energy of almost 23 MeV [23,32].

III. DATA ANALYSIS

The details of the data handling and data analysis of the two Gammasphere experiments have also been described earlier (see, for example, Refs. [24–26] and references therein). In short, the determination of the kind of charged particles detected in the Microball elements as well as the neutron-γ separation in the Neutron-Shell events are based on standard pulse-shape discrimination techniques [29,30,33,34]. For the present experiments, the detection efficiencies amount to $\sim$65% for protons, $\sim$50% for α particles, and $\sim$25% for neutrons. The Doppler correction of the γ-ray events is based on an event-by-event kinematic reconstruction method. It takes into account the measured momentum vectors of the evaporated particles, from which the momentum vector of the recoiling nucleus can be derived. This method significantly reduces the effect of the Doppler broadening caused by the evaporated particles compared to simpler approaches, which are based on an average recoil velocity in beam direction.

The γ-ray events were subsequently selected by appropriate conditions on the number of and kind of evaporated particles and incremented into various E_γ projections and E_γ-E_γ matrices. In the case of ^{54}Co, the analysis focused on γ rays detected in coincidence with one α particle, one proton, and one neutron ($1\alpha 1p1n$). The associated spectra and matrices were investigated with the RADWARE software package [35] and the spectrum-analysis code Tv [36] to construct the level scheme and derive the relative intensities of the γ-ray transitions.

Since ^{54}Co is a weak reaction channel, the raw $1\alpha 1p1n$ γ-ray spectra and matrices comprise significant contributions from the much more intense $1\alpha 2p1n$ reaction channel ^{53}Fe [26] and, less pronounced, from the $1\alpha 3p1n$ channel ^{52}Mn, from the $2\alpha 1p1n$ channel ^{50}Mn, as well as from ^{51}Mn ($2\alpha 1p$), ^{53}Mn ($1\alpha 3p$), ^{55}Fe ($4p1n$), and ^{56}Co ($3p1n$). The former three contaminations arise from events when one or more charged particles escaped the detection in Microball. The latter are due to misidentified protons and α particles and small ($<$0.1%) ^{29}Si target impurities. All these contaminants can be suppressed considerably by applying the total energy plane selection method [28] and by eventually subtracting carefully γ-ray spectra in coincidence with, for example, one α particle, *two* protons, and one neutron.

Figure 1 compares the total projections of the $\gamma\gamma$ correlation matrices in coincidence with one α particle, one proton, and one neutron (black) and in coincidence with one α particle, two protons, and one neutron (gray). Both matrices and spectra are purified by means of the above-mentioned total energy plane selection method, which is optimized for known transitions in ^{54}Co [3,19] and ^{53}Fe [26], respectively. The two spectra are normalized with respect to the background level at about 3.0-MeV γ-ray energy. Gray peak labels denote known

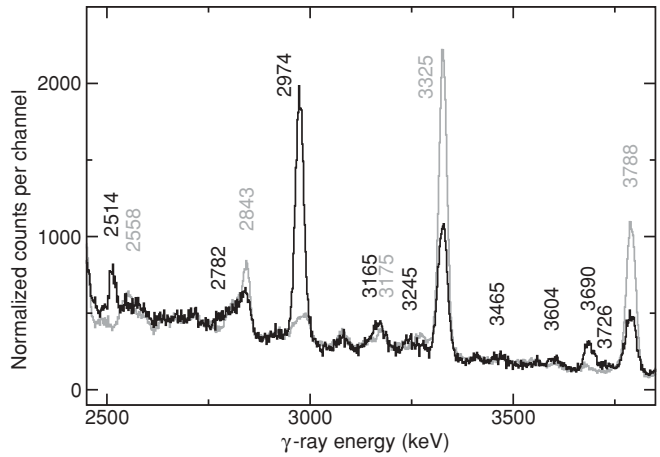

FIG. 1. Normalized total projections of the $\gamma\gamma$ matrices in coincidence with one α particle, one proton, and one neutron (black) and in coincidence with one α particle, two protons, and one neutron (gray). Both matrices and spectra are purified by means of the total energy plane selection method [28]. Energy labels are in keV and correspond to transitions in ^{54}Co (black) and ^{53}Fe [26] (gray).

high-energy γ-ray transitions in ^{53}Fe, while black peak labels mark known (2514 and 2974 keV [3]) or new transitions found to belong to ^{54}Co. The latter are based on excess counts in the black spectrum relative to the gray spectrum in Fig. 1 and possibly confirmed by $\gamma\gamma$ coincidence relations (cf. Sec. IV).

Multipolarity assignments of transitions are mainly based on ratios of yields R_{150-97}. This is the ratio of efficiency-corrected γ-ray intensities measured in the three most backward rings of Gammasphere (average angle $\overline{\theta} = 150^\circ$ with respect to the beam axis) versus the central section of Gammasphere ($\overline{\theta} = 97^\circ$) [3]. The ratios were evaluated from γ-ray spectra taken in coincidence with proper particle gates (cf. Fig. 1) and intense transitions known to belong to ^{54}Co. These transitions were detected at an average angle of $\overline{\theta} = 124^\circ$, where the relative intensities from different multipolarities are about the same. Stretched quadrupole transitions should reveal $R_{150-97} \sim 1.2$–1.3, whereas stretched dipole transitions are predicted to have $R_{150-97} \sim 0.8$. Significantly smaller or larger values indicate mixed $\Delta I = 1$, $E2/M1$ transitions. Pure nonstretched ($\Delta I = 0$) dipole transitions have values similar to quadrupole transitions. Often, the two cases can be distuinguished due to parallel decay branches or with the help of yrast arguments, i.e., states along the yrast line are more strongly populated than off-yrast levels in fusion-evaporation reactions.

IV. RESULTS

The experimental results are summarized in the level scheme presented in Fig. 2 and Table I. Table I provides level energies, γ-ray transition energies, relative γ-ray intensities, and R_{150-97} values together with suggested spins and parities of initial and final states for ^{54}Co.

In the previous heavy-ion fusion-evaporation study of ^{54}Co [3] the 1557-, 1876-, and 2514-keV transitions were found to be in coincidence with an intense line at 2974 keV, which was placed on the β-decaying 7^+ state at 197 keV [16]. This assignment is confirmed with the present data (cf. Fig. 1 for the 2514- and 2974-keV lines) and corresponding $\gamma\gamma$ coincidence relationships.

The central section of the proposed excitation scheme of ^{54}Co in Fig. 2 is by and large revealed by the γ-ray spectrum taken in coincidence with the 1557-keV line. This is shown in Fig. 3(a). Next to the known 2514- and 2974-keV lines a relatively intense peak is observed at 3690 keV and two more at 2068 and 3245 keV, respectively. Not only is the 3690 keV line also clearly visible in the black spectrum of Fig. 1, but the sum $3690 + 2068$ equals $2514 + 3245$ within uncertainties. Underpinned by the corresponding $\gamma\gamma$ coincidences and using the associated R_{150-97} values, the yrast sequence up to the tentative $I^\pi = 14^+$ state at 10486 keV can be easily established.

The right-hand section of Fig. 3(a) provides four high-energy peaks at 4961, 5266, 5524, and 5779 keV. All four transitions are found to be in sole coincidence with the 2974- and 1557-keV lines, i.e., feeding the 11^+ level at 4728 keV. This is exemplified in Fig. 3(b), which is the coincidence spectrum of the 5524-keV transition. Note also that it is empty

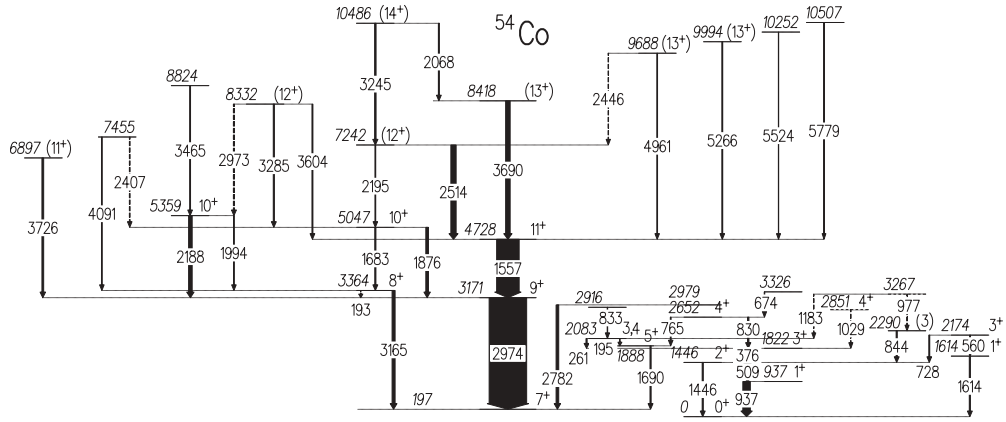

FIG. 2. Partial decay scheme of ^{54}Co from the present study. Energy labels are in keV, and the widths of the arrows correspond to the relative intensities of the γ rays. Tentative levels and transtions are dashed.

TABLE I. Summary of the experimental results on excited states and γ rays associated with ^{54}Co observed in the present work: Energies, spins, and parites of the excited states and transition energies, relative intensities, and angular distribution ratios of the γ rays.

E_x (keV)	E_γ (keV)	$I_{\rm rel}$ (%)	R_{150-97}	Multipolarity	J_i^π ($\hbar$)	J_f^π ($\hbar$)
937(1)	937(1)	20(2)	0.91(10)	$\Delta I = 1$	1^+[a]	0^+
1446(1)	509(1)	18(1)	0.87(8)	$\Delta I = 1$	2^+[a]	1^+
	1446(1)	3(1)			2^+	0^+
1614(1)	1614(2)	3(1)[b]			1^+[a]	0^+
1822(1)	376(1)	11.6(5)	0.88(9)	$\Delta I = 1$	3^+[a]	2^+
1888(2)	1690(2)	3(1)[b]			5^+[a]	7^+
2083(2)	195(1)	0.9(3)			3, 4[a]	5^+
	261(1)	3.0(4)	0.95(21)	$\Delta I = 0, 1$	3, 4	3^+
2174(1)	560(1)	2.4(5)[c]			3^+[a]	1^+
	728(1)	2.5(4)			3^+	2^+
2290(2)	844(1)	3.0(4)	1.07(33)	$\Delta I = 0, 1$	(3)[a]	2^+
2652(2)	765(1)	2.1(5)[c]			4^+[a]	5^+
	830(1)	3.7(8)	0.99(23)[d]	$\Delta I = 0, 1$	4^+	3^+
2851(2)	1029(1)	0.7(2)			4^+[a]	3^+
2916(2)	833(1)	1.2(4)				3, 4
2979(5)	2782(5)	7(1)				7^+
3171(3)	2974(2)	100(4)	1.30(12)	$E2$	9^+	7^+
3267(2)	977(1)	0.9(2)				(3)
	1183(2)	0.5(2)				(3)
3326(2)	674(1)	1.4(3)				4^+
3364(3)	193(1)	1(1)			8^+	9^+
	3165(3)	8(1)	1.26(36)	$E2/M1$	8^+	7^+
3794(5)	3597(5)	3(1)				7^+
4728(3)	1557(1)	60(3)	1.25(9)	$E2$	11^+	9^+
5047(3)	1683(1)	3(1)			10^+	8^+
	1876(1)	7.0(6)	1.21(19)	$\Delta I = 0, E2/M1$	10^+	9^+
5359(3)	1994(2)	2(1)			10^+	8^+
	2188(1)	9.5(8)	0.48(11)	$E2/M1$	10^+	9^+
6897(4)	3726(3)	4.6(7)	1.62(56)	$(E2)$	(11^+)	9^+
7242(4)	2195(2)	2(1)			(12^+)	10^+
	2514(2)	14(2)	0.98(10)	$(E2/M1)$	(12^+)	11^+
7455(5)	2407(2)	2(1)				10^+
	4091(4)	2(1)				8^+
8332(5)	2973(3)	3(2)			(12^+)	10^+
	3285(3)	3(1)			(12^+)	10^+
	3604(4)	2.5(4)	0.88(18)	$(\Delta I = 1)$	(12^+)	11^+
8418(4)	3690(3)	12(1)	1.22(13)	$E2$	13^+	11^+
8824(4)	3465(3)	2.3(6)				10^+
9688(4)	2446(2)	1.3(5)			(13^+)	(12^+)
	4961(4)	1.9(4)	1.43(46)	$(E2)$	(13^+)	11^+
9994(5)	5266(4)	2.3(4)	1.26(44)	$(E2)$	(13^+)	11^+
10252(6)	5524(5)	0.8(3)				11^+
10486(4)	2068(1)	2.7(5)	0.91(22)	$(E2/M1)$	(14^+)	13^+
	3245(3)	3.8(8)	1.27(23)	$(E2)$	(14^+)	(12^+)
10507(8)	5779(7)	0.3(1)				11^+

[a]Adopted from or consistent with Ref. [16].
[b]Estimated from the summed intensity of feeding transitions.
[c]Derived from known branching ratio [16,19].
[d]Doublet structure.

besides the two peaks of the main high-spin cascade in ^{54}Co, which is in fact the case for any of these four high-energy lines. For two of them the R_{150-97} values can be deduced consistent with quadrupole character. Therefore, the 9688-, 9994-, 10 252-, and 10 507-keV states form a series of yrare 13^+ states.

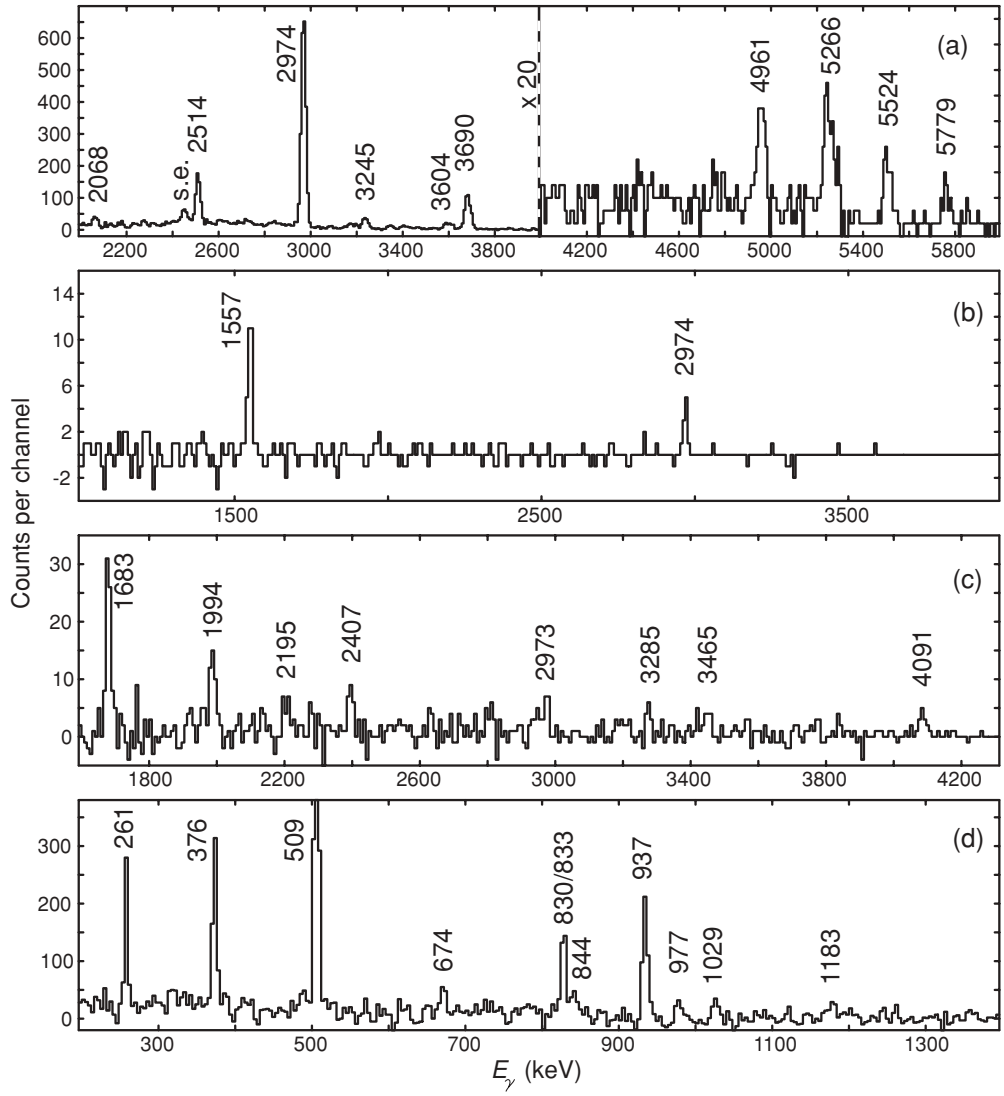

FIG. 3. Gamma-ray spectra taken in coincidence with one α particle and one proton detected in Microball [29] and one neutron in the Neutron Shell [30]. Summed particle- and γ-ray energy requirements adjusted for ^{54}Co have also been imposed. Parts (a), (b), and (c) are binned 8 keV per channel, whereas part (d) is binned 4 keV per channel. Peak energy labels are in keV. The label s.e. indicates the single-escape peak of the 2974-keV transition. Part (a) is in coincidence with the 1557-keV, $11^+ \rightarrow 9^+$ yrast transition. Part (b) is coincidence with the 5524-keV high-energy line feeding the 11^+ state at 4728 keV. Part (c) illustrates the left-hand side of the ^{54}Co decay scheme in Fig. 2. The spectrum is in coincidence with the 3165-keV $8^+ \rightarrow 7^+$ yrast transition. Finally, part (d) illustrates the low-spin portion of the level scheme of ^{54}Co (cf. Fig. 2 and Ref. [19]) as seen in the present experiment. The spectrum represents the sum of the spectra in coincidence with the 937-keV ground-state transition and the 376-keV $3^+ \rightarrow 2^+$ yrast transition.

The only transition remaining in Fig. 3(a) is the one at 3604 keV. Once more there is also in excess of counts in the black spectrum of Fig. 1, and it is found to be consistent with a dipole transtion to connect a tentative 12^+ state at 8332 keV with the yrast sequence. The left-hand side of Fig. 2 is further described by the γ-ray spectrum in Fig. 3(c), which is taken in coincidence with the new 3165-keV transition. It is placed parallel to the 2974-keV transition. Peaks at both 1683 and 1994 keV are clearly visible in Fig. 3(c). These two transitions couple the two 10^+ states at 5047 and 5359 keV with the 3165-keV transition, while in particular the R_{150-97} values of the 2188-keV line defines the associated spins and parities, in conjunction with the values derived for the above-mentioned 1876- and 3604-keV transitions. The spectrum in Fig. 3(d) illustrates the low-spin scheme build mainly on top of the 0^+ ground state of ^{54}Co. This part is relatively weakly populated in the present experiments and supports and confirms the more dedicated study of Ref. [19].

Nevertheless, there is one potentially important supplement in our data set, namely the new high-energy transition at 2782 keV. First, there is a clear excess of counts at that energy in Fig. 1, in particular with respect to a number of weaker transitions such as the ones at 3165, 3245, 3465, or 3604 keV, which were readily established in the excitation scheme of ^{54}Co by means of $\gamma\gamma$ coincidences. Second, with the present data set it is impossible to establish coincidences

for the 2782-keV line with any of the intense lines known to belong to ^{54}Co, either on the high-spin side (1557, 2974, or 3165 keV) or on the low-spin side (376, 509, or 937 keV). Third, no γ rays are observed to possibly connect it further to the two 10^+ states, which would be in close resemblance to the 1683-, 1994-, and 3165-keV scheme. Note that this "single" 2782-keV transition can pass the experimental event trigger conditions due to (unresolved) coincidences with γ rays from both the continuum and (unknown) discrete states in ^{54}Co. Last but not least, the 2782-keV transition was not observed in the low-spin study of Ref. [19] either, i.e., the spin value of the initial state should be at least 5 $\hbar$. The combination of these arguments leads us to suggest that the 2782-keV transition marks the decay of a medium-spin yrast 6^+ state positioned at 2979 keV into the 7^+ state at 197 keV. However, since we cannot establish angular distribution information of the 2782-keV line because of the lack of statistics, the 6^+ spin-parity assignment cannot be established (though likely). Therefore, the 2979-keV state remains unlabeled in Fig. 2.

V. DISCUSSION

A. Spherical shell-model calculations

Spherical large-scale shell-model calculations were performed using the shell-model code ANTOINE [37,38] to interpret the observed excitation scheme of ^{54}Co. The full fp space is considered, i.e., the $1f_{7/2}$ orbital below and the $2p_{3/2}$, $1f_{5/2}$, and $2p_{1/2}$ orbitals above the $N = Z = 28$ shell closure are included for both protons and neutrons. For the present results, the shell-model space is truncated to allow up to $t = 6$ particles (protons or neutrons) to be excited across the shell gap at particle number 28. This is considered a compromise between available computing power and sufficient convergence of the calculated numbers for the near-spherical states [4]. Both the KB3G [39] and GXPF1A [40,41] effective interactions have been considered, the predictions of which are generally very reliable for mass $A \sim 50$ nuclei [4,5,42,43].

The influence of isospin-breaking terms on predictions of in particular the proton-neutron $1f_{7/2}{}^{-2}$ multiplet of ^{54}Co (cf. Ref. [21]) is studied by incorporated isospin-breaking terms into the KB3G shell-model parametrization (KB3G-IB in the following) along the scheme outlined in Ref. [43]. In the standard notation [5,15,43], these include (i) multipole harmonic-oscillator Coulomb matrix elements, $V_{\rm CM}$; (ii) the monopole electromagnetic spin-orbit interaction, $V_{\rm Cls}$; (iii) the addition of monopole radial effects; and (iv) the $T = 1$, $J = 2$ matrix element of the effective interaction for two protons has been increased by +100 keV. This isospin-breaking term, usually denoted $V_{\rm BM}$, has been introduced by Zuker *et al.* [15] based on mass $A = 42$ mirror-pair energies, recently confirmed by a mirror-energy study of the $A = 54$ isobars ^{54}Fe and ^{54}Ni [18].

To describe the electromagnetic decay properties, effective charges of $e_{{\rm eff},p} = 1.15$ and $e_{{\rm eff},n} = 0.80$ derived in Ref. [44] for $N \sim Z$ nuclei near ^{56}Ni are used as well as free gyromagnetic factors.

TABLE II. Experimental and predicted branching ratios of selected high-spin states ($I_i \geqslant 8$) in ^{54}Co. Only observed or predicted transitions beyond the present experimental detection limit are included. The note n.o. thus implies predicted but nonobserved transitions. Experimental transition energies have been used in the comparison.

E_x (keV)	E_γ (keV)	I_i ($\hbar$)	I_f ($\hbar$)	$b_{\rm exp}$ (%)	$b_{\rm theo}$ (%)	
					KB3G	GXPF1A
3364	193	8^+	9^+	11(11)	0	0
	3165		7^+	89(11)	100	100
4728	1557	11^+	9^+	100	100	100
5047	1683	10^+	8^+	30(8)	31	50
	1876		9^+	70(8)	69	49
5359	1994	10_2^+	8^+	17(8)	27	32
	2188		9^+	83(8)	73	68
6897	1538	(11_2^+)	10_2^+	n.o.	37	0
	2169		11^+	n.o.	34	1
	3726		9^+	100	1	97
7242	1883	(12^+)	10_2^+	n.o.	5	8
	2195		10^+	12(7)	0	0
	2514		11^+	88(7)	95	92
8332	2973	(12_2^+)	10_2^+	35(23)	0	25
	3285		10^+	35(15)	21	17
	3604		11^+	30(10)	78	56
8418	3690	13^+	11^+	100	100	98
9688	1356	(13_2^+)	(12_2^+)	n.o.	27	0
	2446		(12^+)	41(14)	26	0
	4961		11^+	59(14)	38	94
9994	5266	(13_3^+)	11^+	100	98	96
10252	5524	$[13_4^+]$[a]	11^+	100	90	29
10486	2068	(14^+)	13^+	42(9)	73	70
	3245		12^+	58(9)	25	26

[a]Taken from the shell-model calculation.

1. *High-spin states*

Table II and Fig. 4 summarize and illustrate the comparison of the experimental results in the high-spin sector of the excitation scheme of ^{54}Co with the shell-model calculations. Apparently the KB3G interaction yields consistently too high excitation energies, while on the other hand they are predicted consistently too low in the case of GXPF1A. In essence independent of whether they are odd- or even-spin yrast states or yrare states, the experimentally observed states lie in between the predictions of the two interactions. Based on that, yrast arguments, and restrictions due to known spins and parties of the final states of their γ decay pattern, the states at 8824, 10252, and 10507 keV can be associated with the 12_3^+, 13_4^+, and 13_5^+, respectively. Though energetically properly located, the 7455-keV state cannot be mapped with the calculated 11_3^+ state, since it decays into the 8^+ 3364-keV level. Thus it is likely to either represent a 10^+ state of higher rank or possibly a negative-parity state.

The assignment of these high-spin states is further underpinned by the predicted branching ratios, which are presented in Table II. With the exceptions of the predictions for the 11_2^+ state in case of KB3G and possibly the 13_2^+ state in case of GXPF1A, the observed decay scheme is reproduced

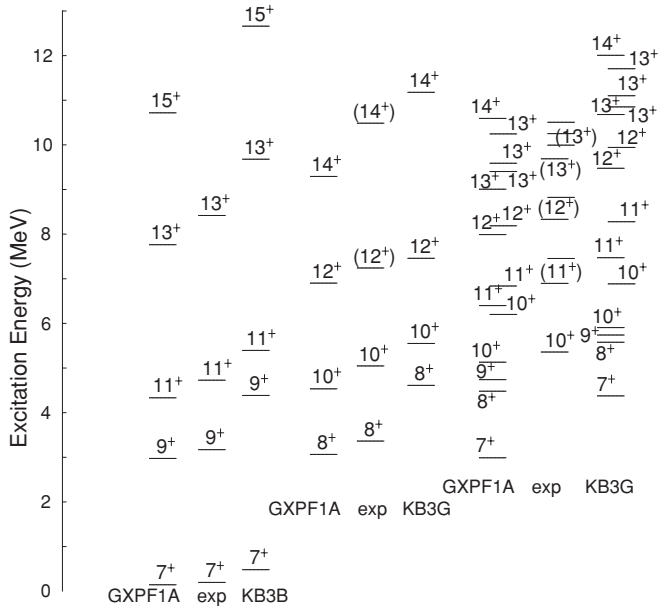

FIG. 4. Comparison of observed and predicted high-spin states in ^{54}Co. They are grouped in odd-spin and even-spin yrast as well as yrare states (from left to right). The results using two different effective interactions (KB3G and GXPF1A) are presented.

more or less one-to-one, in particular when recalling the present observational limits for high-energy γ-ray transitions. State lifetimes are predicted to less than a few hundred femtoseconds for most of these states. Only the yrast 10^+ ($\tau \sim 2.8$ ps) and 11^+ ($\tau \sim 1.0$ ps) mark a slight difference, but consistently for both interactions used. Interestingly, rather large mixing ratios $\delta(E2/M1)$ are predicted for a number of $\Delta I = 1$ transitions; examples with reasonable yield are the 3165-keV $8^+ \rightarrow 7^+$, the 2188-keV $10^+_2 \rightarrow 9^+$, or the 2514-keV $12^+ \rightarrow 11^+$ transitions. Especially for the former two this is supported by their experimental angular distribution ratios, which differ significantly from the values expected for pure dipole transitions.

2. The 2979-keV state

The $T = 1, 6^+$ state is of specific interest as to complement both studies of the $A = 54$ isobaric triplet as well as concluding discussion on cross-conjugate symmetries in the $1f_{7/2}$ shell in conjunction with the $A = 42$ triplet [15]. Based on the present experimental data a state at 2979-keV excitation energy forms a candidate for that state in ^{54}Co.

Table III provides some predictions on $6^+_{1,2}$ and 7^+_2 states using the different shell-model parametrizations. These three calculated states are the candidates to be associated with the observed 2979-keV level, which experimentally decays exclusively into the 7^+_1 state via the 2782-keV transition. First, the inclusion of isospin-breaking terms does not alter the picture, except for some minor changes in the excitation energy, the predictions of KB3G and KB3G-IB are essentially the same. The predicted isospin $T = 1$, 6^+ state is easily discriminated by the large $\Delta T = 1$, $B(M1; 6^+ \rightarrow 7^+_1)$ (cf. Table III) and $B(M1; 6^+ \rightarrow 5^+_1)$ values. Both interactions place this predominantly $1f_{7/2}{}^{-2}$ state at a similar excitation energy around 3 MeV, which is in line with the observations for other low-spin yrast states, for which both interactions also yield very comparable excitation energies. Moreover, all calculations predict a $\sim$10% branch into the $T = 0$, 5^+ state. Experimentally, this branch gives rise to a possible 1091- to 1690-keV cascade (cf. Fig. 2), though not observed in the present data. Note, however, that the relative yield of the predicted 1091-keV line is less than 1% in the units of Table I. This weak 1091-keV line could only be discriminated via a coincidence with the 1690-keV transition, but the cascade falls below the present observational limit, not least because of the low yield and relatively high transition energy of the known 1690-keV line. In turn, the $T = 0$, 6^+ state and the 7^+_2 state are calculated to exclusively decay into the yrast 7^+ state; consistently for both interactions. Since these states comprise main partitions with excitations across the shell gap, the energy predictions follow the scheme of the high-spin states (cf. Fig. 4), namely $E_{x,\mathrm{theo}}(\mathrm{GXPF1A}) - E_{x,\mathrm{theo}}(\mathrm{KB3G}) \sim 1$ MeV.

While the 7^+_2 assignment is somewhat more unlikely due to its predicted higher average excitation energy, both calculated 6^+ states remain good choices for the observed level at 2979 keV. A dedicated medium-spin experiment could shed light on the weak but anticipated 1091- to 1690-keV coincidence and eventually determine the $\delta(E2/M1)$ mixing ratio of the 2782-keV line: This is expected close to zero in case it depopulates the $T = 1, 6^+$ state of the $1f_{7/2}{}^{-2}$ multiplet, while $|\,\delta\,| \gg 0$ is predicted for the other two options.

3. Notes on the low-spin states

The dedicated low-spin investigation presented in Ref. [19] was based on the ^{54}Fe$(p, n\gamma)^{54}$Co reaction. It is thus much more sensitive to the observation of low-spin nonyrast states than the fusion-evaporation access used in our study, which favors the population of medium- to high-spin states in ^{54}Co.

TABLE III. Characteristics of the calculated 6^+_1, 6^+_2, and 7^+_2 states, which can possibly account for the new level at 2979 keV.

	KB3G				KB3G-IB				GXPF1A			
I_i ($\hbar$)	E_x (keV)	$B(M1; I_i \rightarrow 7^+_1)$ ($\mu_N{}^2$)	$b(7^+_1)$ (%)	$b(5^+_1)$ (%)	E_x (keV)	$B(M1; I_i \rightarrow 7^+_1)$ ($\mu_N{}^2$)	$b(7^+_1)$ (%)	$b(5^+_1)$ (%)	E_x (keV)	$B(M1; I_i \rightarrow 7^+_1)$ ($\mu_N{}^2$)	$b(7^+_1)$ (%)	$b(5^+_1)$ (%)
6^+_1	3022	0.86	88	12	3039	0.89	88	12	2565	0.00	99	0
6^+_2	3790	0.00	99	0	3644	0.00	99	0	2904	0.76	90	9
7^+_2	4375	0.00	100	0	4185	0.00	100	0	2989	0.00	100	0

FIG. 5. Comparison of observed and predicted low-spin states in ^{54}Co. They are grouped according to the different spin values. The results of two different interactions (KB3G and GXPF1A) are included, as well as KB3G modified with isospin-breaking terms (−IB) [43].

Nevertheless, the two methods nicely complement each other. Not only is the low-spin part shown on the right-hand side of Fig. 2 fully consistent with the level scheme derived in Ref. [19], but it is also selective: Levels missing in Fig. 2 but seen in Ref. [19] are likely to represent low-spin nonyrast states.

Figure 5 illustrates the energy correlations between observed and predicted low-spin levels, while Table IV provides information on some associated decay branches. Looking at the states dominated by the $1f_{7/2}{}^{-2}$ multiplet (0^+_1, 1^+_1, 2^+_1, 3^+_1, 4^+_2, and 5^+_1), the KB3G calculation provides excellent agreement in terms of excitation energies, which is even slightly improved when including the isospin-breaking effects. At variance, GXPF1A predicts the 1^+, 3^+, 4^+, and 5^+ states of the multiplet some 400 keV below the 0^+, 2^+, and 7^+ states of the multiplet (see also Fig. 4). The same is true for the yrast 4^+ state, which must be associated with the level at 2083 keV: Experimentally it is marked with spin $I = 3, 4$ [16,19], and it decays into the yrast 3^+ and 5^+ states with two low-energy transitions. All calculated 3^+ states find their experimental counterparts up to some 3-MeV excitation energy, while the $T = 0$-dominated yrast 4^+ state comes below the $T = 1$, 4^+ state of the $1f_{7/2}{}^{-2}$ multiplet in the present calculations once more than three particles are allowed to be excited into the upper fp shell ($t > 3$), irrespective which interaction is used. The only experimental level left to be associated with the yrast 4^+ state is thus the one at 2083 keV. The predicted branching ratios of the 2083-keV state are in nice agreement with experiment, in particular given the rather small $B(M1)$ and $B(E2)$ rates, which make the level isomeric on the nanosecond scale in the calculations. Actually, KB3G-IB yields the best prediction for the 2083-keV state.

TABLE IV. Experimental and predicted branching ratios of selected low-spin states ($I_i \geqslant 6$) in ^{54}Co. Only observed or predicted transitions beyond the present experimental detection limit are included, and whenever possible, results from Ref. [19] and the present data have been merged. The note n.o. thus implies predicted but nonobserved transitions. Experimental transition energies have been used in the comparison.

E_x (keV)	E_γ (keV)	I_i ($\hbar$)	I_f ($\hbar$)	$b_{\rm exp}$ (%)	$b_{\rm theo}$ (%)		
					KB3G	KB3G-IB	GXPF1A
1446	509	2^+	1^+	88(3)	94	94	92
	1446		0^+	12(3)	6	4	8
1614	1614	1^+_2	0^+	100	100	100	98
1822	376	3^+	2^+	98(1)	99	99	99
	885		1^+	2(1)	1	1	1
1888	1690	5^+	7^+	100	100	100	100
2083	195	$[4^+]$[a]	5^+	26(3)	59	39	54
	261		3^+	74(3)	41	61	46
2149	1952	5^+_2[b]	7^+	100	100	100	100
2174	560	3^+_2	1^+_2	38(5)	9	0	56
	728		2^+	40(5)	91	99	33
	1237		1^+	22(4)	0	1	11
2290	676	$[3^+_3]$[a]	1^+_2	n.o.	0	10	50
	844		2^+	100	99	90	48
2652	765	4^+_2	5^+	34(2)	37	37	29
	830		3^+	66(2)	63	63	70
2851	561	4^+_3[b]	3^+_3	n.o.	20	0	1
	677		3^+_2	n.o.	1	6	0
	702		5^+_2	n.o.	38	11	1
	768		4^+_1	n.o.	13	3	1
	965		5^+	36(1)	18	17	30
	1029		3^+	66(2)	11	62	68

[a]Taken from the shell-model calculation.
[b]Taken from Ref. [19].

For the remaining yrare states the situation is comparable to the high-spin states depicted in Fig. 4; GXPF1A provides consistently too low but levels lying rather closely to the experimental ones, while it is the opposite for KB3G. The wave functions of the predicted 3^+_2 and 3^+_3 states had to be exchanged for KB3G to provide the proper description of the branching ratios of these states (cf. Table IV). This deficiency could be cured by using KB3G-IB, which notably improved the level of agreement with experiment in essentially all cases, i.e., KB3G-IB is superior to KB3G in describing the low-spin regime of ^{54}Co. There are also levels in the experimental schemes of Ref. [19] and Fig. 2 which can be readily associated with, for example, the second 2^+ state (2657 keV), the fourth 4^+ state (3267 keV), or the third and fourth 5^+ states (2916 and 3326 keV).

Table V provides some additional information on $\delta(E2/M1)$ mixing ratios of isovector and isoscalar dipole transitions depopulating the three lowest 4^+ states in ^{54}Co. Note that the simple two-state mixing scheme illustrated in

TABLE V. Selected experimental [21] and predicted mixing ratios $\delta(E2/M1)$ of $\Delta I = 1$ transitions depopulating $I^\pi = 4^+$ states. Experimental transition energies have been used in the comparison.

E_x (keV)	E_γ (keV)	I_i ($\hbar$)	I_f ($\hbar$)	$\delta_{\rm exp}$	$\delta_{\rm theo}$	
					KB3G	KB3G-IB
2083	261	4_1^+	3^+		0.57	−0.06
	195		5^+		24	−0.18
2652	830	4_2^+	3^+	0.00(3)	0.00	0.00
	765		5^+		0.00	0.00
2851	1029	4_3^+	3^+	0.12(4)	0.47	0.10
	965		5^+		−1.40	0.39

Fig. 1 of Ref. [21] is not necessarily valid anymore, since the dominantly $T = 1, 4^+$ state at 2652 keV is embedded in two (or more) dominantly $T = 0, 4^+$ states at 2083 and 2851 keV. Of course, the basis of the isospin mixing analysis of Ref. [21], i.e., a detailed analysis of $\delta(E2/M1)$ mixing ratios, is still valid. Eventually it needs to be expanded to a three- or four-state mixing model, and the numerical result on isospin mixing may require a dedicated cross-check using full fp shell-model calculations. In fact, even the present $t = 6$ approach may not be sufficient. At $t = 6$ GXPF1A predicts almost degenerate $T = 1$, 4_2^+ and $T = 0$, 4_3^+ states (cf. Fig. 5). Despite the excellent description of the associated branching ratios (cf. Table IV), the degeneracy prevents a meaningful yet simplified two-state mixing approach of these two states. Nevertheless, applying Eq. (6) of Ref. [21] to the $t = 6$ predictions for transition matrix elements from the KB3G interaction for the neighboring $T = 1, 4_2^+$ and $T = 0, 4_3^+$ states, an isospin mixing value of $0.11(^{21}_{6})$ is obtained, which is in line with Ref. [21]. Interestingly, the inclusion of isospin-breaking terms in the $t = 6$ KB3G predicition cures its problems in describing the decay pattern of the $T = 0$, 4_3^+ state, as can be seen from Table IV. Moreover, the measured mixing ratio of the isoscalar 1029-keV, $4_3^+ \rightarrow 3_{+1}$ transitions is readily reproduced with the isospin-broken interaction KB3G-IB; see Table V. Note finally that, comparing the columns for KB3G and KB3G-IB in Table V, the breaking of isospin symmetry can imply drastic changes to specific spectroscopic predictions such as mixing ratios, which hence become sensitive observables to isospin-breaking effects.

B. Rotational bands?

Clearly, high-spin rotational bands originating from well- or superdeformed nuclear shapes are absent in the ^{54}Co level scheme shown in Fig. 2. This seems surprising up front, in particular when considering that about the same phase space for the population of high-spin states is accessible in the present fusion-evaporation reaction ^{28}Si(^{32}S,$1\alpha 1p1n$)^{54}Co and the reaction ^{28}Si(^{36}S,$1\alpha 1p1n$)^{58}Cu, in which an intense and very regular rotational band has been observed with a relative yield of some 30% of the ground-state transitions [23].

Experimentally, there are essentially two possibilities explaining the nonobservation of rotational structures in ^{54}Co with the present data. The first option concerns particle decays competing with γ-ray emission from both deformed or spherical high-spin states. Indeed, discrete-energy proton and α "linking transitions" between well-deformed rotational states in the mother nucleus and near-spherical states in the respective daughter nucleus have been observed in nearby nuclei, e.g., proton decays from bands in ^{56}Ni [3,45] and ^{58}Cu [23,46], or α decays from two rotational states in ^{58}Ni [47,48], while principally, of course, any excited state above particle threshold may exhibit particle decay branches, deformed or not. For instance, in case of rotational bands populated via fusion-evaporation reactions, this has been studied by Døssing and coworkers [49], while the hindrance factor induced for the specific proton decay from the deformed band in ^{58}Cu [46] has been explained by a combination of the change of the nuclear shape and the change of the K quantum number of a $1g_{9/2}$ neutron "spectator" [50].

According to Ref. [51] the proton separation energy of ^{54}Co is $S_p = 4353.2(16)$ keV, and the α-decay Q value amounts to $Q_\alpha = 7807.6(9)$ keV. In addition, there is a low-lying, $I^\pi = 19/2$ isomeric high-spin state known in the proton-daughter ^{53}Fe at 3040.4(3) keV excitation energy [52], and there is a low-lying, isospin $T = 0$, $I^\pi = 5^+$ state at 229(7) keV in ^{50}Mn [53]. Excited states and their γ-decay pattern are established for both nuclei as well [26,54]. Assuming energy relations and decay modes of those indicated above [23,47], deformed $I^\pi = 13^+$ or 14^+ states at 10-MeV excitation energy in ^{54}Co could proton decay with $E_p \sim 2.6$ MeV into the isomeric state of ^{53}Fe. Alternatively, 14^- or 15^+ states at 15-MeV excitation energy in ^{54}Co could α decay with $E_\alpha \sim 7$ MeV into the 5^+ yrast state of ^{50}Mn. Independent of which of them is more likely, both decay modes bare the experimental problem that no prompt γ radiation in the daughters would be in coincidence with them, which makes them very difficult to observe. Nevertheless, a dedicated search for proton decays into near-spherical states of ^{53}Fe and α decays into near-spherical states of ^{50}Mn can be undertaken but proved unsuccessful. Note that other particle-decay branches like deuteron, two-proton, or ^{3}He decay are energetically much more unfavored.

The second explanation for the absence of a rotational cascade in the present excitation of ^{54}Co is that there might be several rotational bands with different configurations at comparable excitation energies, which are possibly also close in energy to some spherical configurations. Such a scenario would bring the yield of the γ-ray transitions from these individual bands or states as well as the connecting transitions below the present observational limit.

To study this option in more detail, cranked Nilsson Strutinsky (CNS) [55–57] and ULTIMATE CRANKER (UC) [58] calculations have been carried out for ^{54}Co. Both models are based on a cranked modified oscillator potential where total energies are calculated in a Nilsson-Strutinsky formalism [59]. Pairing is included in the UC formalism but not in the CNS formalism, which in turn makes it possible to fix configurations in more detail in the CNS formalism. In both calculations, standard parameters [55] for the κ and μ Nilsson parameters have been used. These parameters define the strength of the $\vec{l} \cdot \vec{s}$ and l^2 terms in the modified oscillator potential.

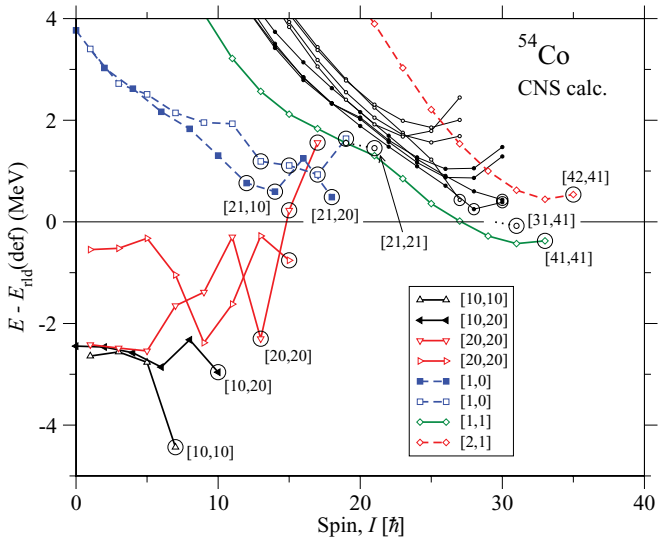

FIG. 6. (Color online) Low-lying configurations of ^{54}Co calculated in the CNS formalism. They are drawn relative to a rotating liquid drop reference as a function of angular momentum, I. Solid (dashed) lines indicate structures with positive (negative) parity. Band-terminating states are encircled.

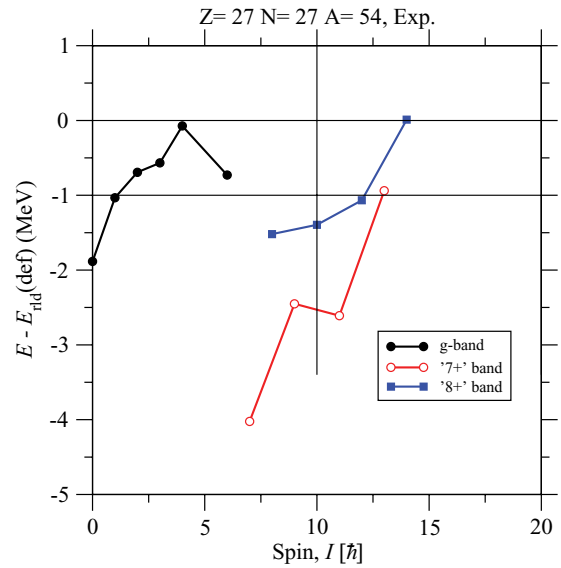

FIG. 7. (Color online) Selected observed states in ^{54}Co drawn relative to the same rotating liquid drop reference as the calculated states in Fig. 6.

1. *Cranked Nilsson Strutinsky assessment*

The energy of the yrast and close-to-yrast states calculated in the CNS formalism are shown in Fig. 6. The low-spin states are labeled as $[p_1p_2, n_1n_2]$, where p_1 (n_1) is the number of proton (neutron) holes of $1f_{7/2}$ character and p_2 (n_2) is the number of $1g_{9/2}$ protons (neutrons). For higher spins it becomes difficult to distinguish between $1f_{7/2}$ holes and particles of $1f_{5/2}$ and $2p_{3/2}$ character (denoted by fp). Hence, these configurations are only labeled as $[p_2, n_2]$. However, selected aligned states are labeled in the more complete way with the spin contribution from the different j shells spelled out in Table VI. Note especially that several terminations may occur in the [1,1] configuration depending on the number of $1f_{7/2}$ holes as exemplified by the aligned [21,21], [31,41], and [41,41] states. Higher-lying excited [1,1] configurations, which are still easy to specify (see below), are drawn by thinner lines in Fig. 6.

Because pairing is neglected in the CNS calculations, no detailed agreement between calculations and experiment is expected at low spin. However, a comparison with the observed states in Fig. 7 shows a general agreement where the rapid decrease of the relative binding energy in the $I = 7$–$14\ \hbar$ spin range is reproduced. According to the calculations, the decrease of relative binding energies continues up to $I \approx 20\,\hbar$ with yrast states, which are mainly noncollective. Several of these yrast states are the terminating highest spin states, I_{max}, in configurations with more and more particles excited across the $Z = N = 28$ gap and subsequently excited into the $\mathcal{N} = 4$, $1g_{9/2}$ subshell. Details of the configurations of some of these aligned states is provided in Table VI, including their deformation parameters. Configurations with a small I_{max} are dominated by holes in the $Z = N = 28$ core leading to prolate shape ($\gamma = -120°$) for these noncollective states, but for larger

TABLE VI. The short hand notation of the maximum spin states of Fig. 6 are specified in the first column. The deformation and spin values of these terminating states are given in the next three columns while their occupation of different subshells relative to the shell gap at particle number 28 and corresponding spin contributions are specified for protons and neutrons in the two last columns.

$[p_1p_2, n_1n_2]$	ε_2(min)	γ(min)	I^{π}_{max}	Proton configuration	Neutron configuration
[10, 10]	0.10	$-120°$	7^+	$\pi(f_{7/2})^{-1}_{7/2}$	$\nu(f_{7/2})^{-1}_{7/2}$
[10, 20]	0.14	$-120°$	10^+	$\pi(f_{7/2})^{-1}_{7/2}$	$\nu(f_{7/2})^{-2}_{6}(fp)^{1}_{1/2}$
[20, 20]	0.18	$-120°$	13^+	$\pi(f_{7/2})^{-1}_{6}(fp)^{1}_{1/2}$	$\nu(f_{7/2})^{-2}_{6}(fp)^{1}_{1/2}$
[21, 10]	0.05	$-120°$	14^-	$\pi(f_{7/2})^{-2}_{6}(g_{9/2})^{1}_{9/2}$	$\nu(f_{7/2})^{-1}_{7/2}$
[21, 20]	0.02	$-120°$	18^-	$\pi(f_{7/2})^{-2}_{6}(g_{9/2})^{1}_{9/2}$	$\nu(f_{7/2})^{-2}_{6}(fp)^{1}_{1/2}$
[21, 21]	0.02	$60°$	21^+	$\pi(f_{7/2})^{-2}_{6}(g_{9/2})^{1}_{9/2}$	$\nu(f_{7/2})^{-2}_{6}(g_{9/2})^{1}_{9/2}$
[31, 41]	0.17	$60°$	31^+	$\pi(f_{7/2})^{-3}_{15/2}(fp)^{1}_{5/2}(g_{9/2})^{1}_{9/2}$	$\nu(f_{7/2})^{-4}_{8}(fp)^{2}_{4}(g_{9/2})^{1}_{9/2}$
[41, 41]	0.19	$60°$	33^+	$\pi(f_{7/2})^{-4}_{8}(fp)^{2}_{4}(g_{9/2})^{1}_{9/2}$	$\nu(f_{7/2})^{-4}_{8}(fp)^{2}_{4}(g_{9/2})^{1}_{9/2}$
[42, 41]	0.20	$60°$	35^+	$\pi(f_{7/2})^{-4}_{8}(fp)^{1}_{5/2}(g_{9/2})^{2}_{8}$	$\nu(f_{7/2})^{-4}_{8}(fp)^{2}_{4}(g_{9/2})^{1}_{9/2}$

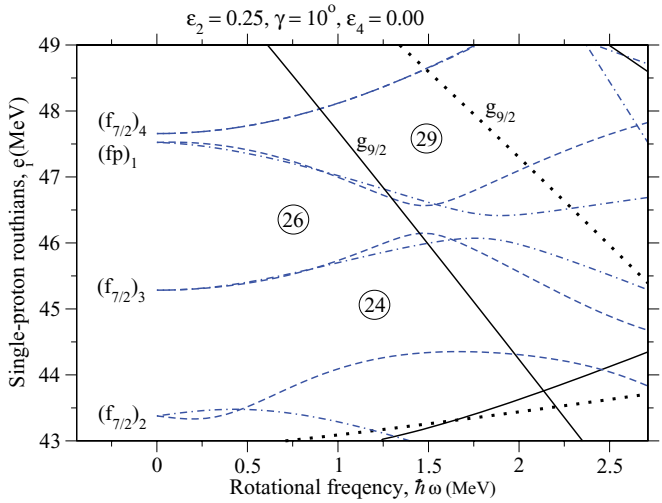

FIG. 8. (Color online) Single-proton Routhians at a typical deformation for ^{54}Co configurations with one $1g_{9/2}$ proton and one $1g_{9/2}$ neutron. The orbitals are labeled according to their dominating j shells and the ordering within their respective groups. fp is used as a shorthand notation for the $1f_{5/2}$ and $2p_{3/2}$ (and $2p_{1/2}$) subshells. Note the crossing between the third $1f_{7/2}$ orbitals and the lowest (fp) orbitals.

values of $I_{\max}$, the fully aligned particles in the $1g_{9/2}$ subshell have a strong driving force toward noncollective oblate shapes ($\gamma = 60^{\circ}$).

It is first with one proton and one neutron excited to the $1g_{9/2}$ subshell that rotational bands with any real collectivity are formed. The single-particle Routhians for protons at a typical deformation for configurations of this type are shown in Fig. 8. Due to the $N = Z$ nature of ^{54}Co, the general features of the corresponding neutron diagram are identical, i.e., this diagram can be used to describe both proton and neutron configurations.

With 27 protons (or neutrons) with one of them in the lowest $1g_{9/2}$ orbital, two of the four orbitals labeled as $(f_{7/2})_3$ and $(fp)_1$ will be occupied. If they have different signatures, the lowest energy configuration at small frequencies will correspond to a configuration with the two $(f_{7/2})_3$ orbitals occupied. Thus in total six $1f_{7/2}$ orbitals are occupied, or equivalently two $f_{7/2}$ orbitals are unoccupied for protons and neutrons. This corresponds to the low-spin range of the [1,1] configuration in Fig. 6, which terminates in the [21,21] state at $I = 21\,\hbar$ (see also Table VI).

In Fig. 8, the $(f_{7/2})_3$ and $(fp)_1$ orbitals come close together and exchange character around $\hbar\omega = 1.5$ MeV. Hence, if the orbitals were followed continuously, the lowest energy configuration would have four $1f_{7/2}$ holes for both protons and neutrons at higher frequency. This is indeed what happens with the [1,1] configuration in Fig. 6, which is seen to terminate in the [41,41] state at $I = 33\,\hbar$.

In the CNS formalism, one tries to create a real crossing between these $(f_{7/2})_3$ and $(fp)_1$ orbitals (removal of virtual interactions), thus making it possible to label the orbitals as being either of $1f_{7/2}$ or (fp) character. One could then further define different configurations with two of these four orbitals occupied leading to six distinct configurations for protons as well as for neutrons, i.e., $6 \times 6 = 36$ total configurations. In the present case, however, the coupling between orbitals of $1f_{7/2}$ or (fp) character appears too strong to remove the virtual interaction at all deformations in a consistent way. With no distinction between the $1f_{7/2}$ and (fp) orbitals, it is only possible to define three configurations of this type for protons and neutrons, respectively. One of them has different signatures for the two particles and two have the same signature for the two particles, namely signature $\alpha = 1/2$ or $\alpha = -1/2$.

The resulting nine configurations are included in Fig. 6. The lowest [41,41] band with "shared signatures" is discussed above while the other eight bands are drawn with thinner lines. One should note that there are 27 additional configurations (or bands) in the energy range of these bands, i.e., within an energy band of approximately 1.5 MeV.

In order to obtain even higher spin values beyond $I = 33\,\hbar$, yet another particle must be excited into the $1g_{9/2}$ subshell. The lowest energy configuration of this kind is provided in Fig. 6 for completeness.

2. *Ultimate Cranker assessment*

To access the influence of pairing correlations on predictions of the observed low to medium spin and characteristics of presumed high-spin rotational bands, calculations using the Ultimate Cranker concept have been performed employing a standard pairing strength [58]. In these calculations, the only conserved quantum numbers are parity, π, and signature, α. A certain quasiparticle configuration can then be given a label like $P(m_p\ n_p)\ N(m_n\ n_n)$, in which case the parity is given by $\pi = (-1)^m$ and the signature by $\alpha = n/2$ for neutrons (n) and protons (p). There are 16 different such configurations since both parity and signature can take two different values. However, a configuration label like $P(m\ n)$ does not uniquely define which quasiparticle levels are occupied, because the same total parity and signature can be obtained in different ways. In the UC calculations the configuration with lowest energy in its parity-signature group at a given spin is chosen at each deformation. Therefore, some excited states may be missing.

In the spin range covered by experiment, i.e., $I < 15\,\hbar$, the UC calculations identify two energetically favorable proton configurations, namely $P(1\ 3)$ and $P(1\ 1)$, i.e., negative parity configurations of both signatures indicating that no proton is excited to the $\mathcal{N} = 4$ shell. In the neutron system, the corresponding configurations are $N(1\ 3)$ and $N(1\ 1)$. At low rotational frequencies, these configurations are one-quasiparticle configurations with the excited quasiparticle in a level originating from the $1f_{7/2}$ subshell. At slightly higher rotational frequencies, a pair of two additional $1f_{7/2}$ quasiparticles will align, forming the three-quasiparticle configuration in the proton system and, correspondingly, in the neutron system.

The proton and neutron configurations can be combined to form the total configurations $P(1\ 3)\ N(1\ 3)$, $P(1\ 3)\ N(1\ 1)$, $P(1\ 1)\ N(1\ 3)$, and $P(1\ 1)\ N(1\ 1)$. These are precisely the four configurations with lowest energy for spin up to $15\,\hbar$ as illustrated in Fig. 9. Their predicted deformation is small, typically $\varepsilon_2 < 0.1$, which is consistent with their description in the previous Secs. V A and V B1. In the UC framework, the "7^+" structure (cf. Fig. 7) can be associated with the $P(1\ 3)$

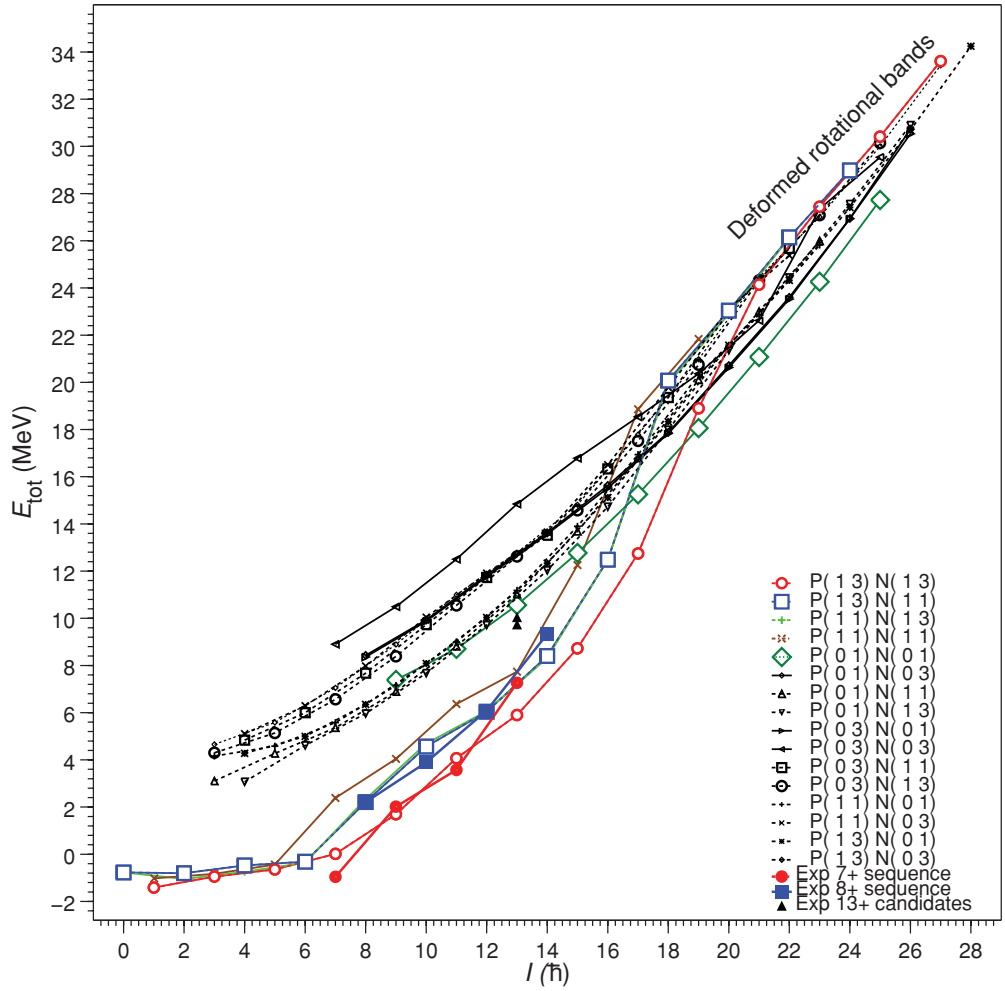

FIG. 9. (Color online) Energies of 16 configurations in the UC framework as function of angular momentum. At high angular momentum ($I > 19\,\hbar$) all configurations correspond to well-developed rotational bands ($\varepsilon_2 \approx 0.3$). At low angular momentum some of the configurations, in particular $P(1\,3)\,N(1\,3)$ (open circles, red online) and $P(1\,3)\,N(1\,1)$ (open squares, blue online), have a lower energy at a small deformation. They are compared to the experimental 7^+ sequence (filled circles, red online) and 8^+ sequence (filled squares, blue online), respectively. Positive-parity configurations are drawn with solid lines, negative-parity configurations with dashed lines. The theoretical energies are given relative to the spherical (nonrotating) liquid drop energy. The experimental energies are shifted by -1.15 MeV such that the energy of the 8^+ state coincides with the energy of the lowest theoretical 8^+ state.

$N(1\,3)$ configuration, while the "8^+" structure may be seen as the lower of the $P(1\,3)\,N(1\,1)$ or $P(1\,1)\,N(1\,3)$ configurations.

The other configurations identified by the UC calculations have at least one proton or one neutron in a $1g_{9/2}$ quasiparticle level, which is strongly deformation driving. In the nonrotating nucleus, the $1g_{9/2}$ level is high above the Fermi surface. Such configurations are thus not favorable at low spin. However, the lowest $1g_{9/2}$ quasiparticle levels align rapidly with increasing rotational frequency and will eventually penetrate the pairing gap. This will favor configurations with one or more $1g_{9/2}$ quasiparticle levels occupied at medium- to high angular momentum. In fact, the proton-neutron symmetric $P(0\,1)\,N(0\,1)$ configuration, which can be described as $\pi g_{9/2} \times \nu g_{9/2}$ is predicted yrast for $I \geqslant 19$ (cf. Fig. 9), in agreement with the [21,21] band and its [41,41] continuation in the CNS approach (cf. Fig. 6). The deformation is found to be large with $\varepsilon_2 \approx 0.3$.

While a well-deformed rotational band with that configuration has been observed in the odd-odd $N = Z = 29$ nucleus ^{58}Cu [23], a corresponding band is not readily seen in the $N = Z = 27$ nucleus ^{54}Co (cf. Fig. 2). The difference is that the calculations for ^{58}Cu predict yrast character already from spin $I = 11\,\hbar$ up to $I \sim 30\,\hbar$. In contrast, the $\pi g_{9/2}\nu g_{9/2}$ band in ^{54}Co is less favorable in energy and, as can be seen from Fig. 9, it competes with several other bands and sequences in the intermediate spin range $I \sim 13$–$19\,\hbar$, i.e., in the regime where the transition from well-deformed rotational bands to near-spherical structures takes place—and in line with that individual transitions can no longer be resolved in the present experimental data (cf. Figs. 2 and 3).

The different positions of the $\pi g_{9/2}\nu g_{9/2}$ bands in ^{58}Cu and ^{54}Co can be understood if one considers that ^{58}Cu has 29 protons and 29 neutrons. Thus, the Fermi surface lies above the magic gap at particle number 28 for both protons and neutrons.

In ^{54}Co, on the other hand, $N = Z = 27$, and the Fermi surface lies below this gap. The $g_{9/2}$ single-particle level is situated above the gap at particle number 28. Consequently, it is closer to the Fermi surface in ^{58}Cu than in ^{54}Co. As a result, the $1g_{9/2}$ quasiparticle level will lie immediately above the pairing gap in the nonrotating ^{58}Cu nucleus and penetrate into the gap as soon as the nucleus starts to rotate. In ^{54}Co, however, the $1g_{9/2}$ quasiparticle level will lie high above the pairing gap at low rotational frequencies, becoming the most favorable quasiparticle level only at higher rotational frequencies and hence angular momenta (see Fig. 9).

VI. SUMMARY

In summary, excited states in the odd-odd $N = Z$ nucleus ^{54}Co have been investigated by means of γ-ray spectroscopic tools. An extended medium-spin excitation scheme of ^{54}Co is deduced from the experimental data.

The results include a strong candidate for the $I = 6$ completion of the $A = 54$ $1f_{7/2}^{-2}$ multiplet observed at 2979-keV excitation energy. Though being consistent with the predictions for both energy and decay path, this level deserves further experimental attention and confirmation, possibly via light-ion induced reactions or pair-transfer studies.

Large-scale spherical shell-model calculations provide an overall good to very good description of the oberved levels and their decay pattern. In addition to the fact that the spherical $N = Z = 28$ gap is somewhat too large for the KB3G interaction compared with GXPF1A, calculations including isospin-breaking terms provide a somewhat better agreement with the experimental data, in particular for decay paths of low-spin states. It is found that the discussion on isospin mixing of neighboring 4^+ states [21] deserves a dedicated revision, i.e., investigations beyond a simple two-state mixing scheme and eventually based on full fp-shell calculations including isospin-breakling terms.

The nonobservation of rotational bands has been explained by cranking calculations with and without pairing. The yrast states up to $I \approx 20\,\hbar$ appear to have very little collectivity with no well-defined rotational bands. The calculations do then suggest a collective yrast band but with a rather high level density just above this yrast band. Furthermore, the input spin is not much higher than $I = 20\,\hbar$. In view of these observations, it is not surprising that it has not been possible to identify any discrete states above $I = 14\,\hbar$ in ^{54}Co.

ACKNOWLEDGMENTS

We thank the accelerator crews and the Gammasphere support staff at Argonne and Berkeley for their supreme efforts. The target maker, Jette Agnete Sørensen, at the Niels Bohr Institute, Copenhagen, Denmark, is also warmly thanked. This work is supported in part by the Swedish Research Council and the US Department of Energy under Grants No. DE-AC03-76SF00098 (Lawrence Berkeley National Laboratory), DE-FG02-88ER-40406 (WU), and DE-AC02-06CH11357 (Argonne National Laboratory).

[1] M. Goeppert Mayer, Phys. Rev. **75**, 1969 (1949).
[2] O. Haxel, J. H. D. Jensen, and H. E. Suess, Phys. Rev. **75**, 1766 (1949).
[3] D. Rudolph *et al.*, Phys. Rev. Lett. **82**, 3763 (1999).
[4] M. Horoi, B. A. Brown, T. Otsuka, M. Honma, and T. Mizusaki, Phys. Rev. C **73**, 061305(R) (2006).
[5] M. A. Bentley and S. M. Lenzi, Prog. Part. Nucl. Phys. **59**, 497 (2007).
[6] G. Kraus *et al.*, Phys. Rev. Lett. **73**, 1773 (1994).
[7] T. Otsuka, M. Honma, and T. Mizusaki, Phys. Rev. Lett. **81**, 1588 (1998).
[8] F. Nowacki, Nucl. Phys. A **704**, 223c (2002).
[9] K. Langanke, J. Terasaki, F. Nowacki, D. J. Dean, and W. Nazarewicz, Phys. Rev. C **67**, 044314 (2003).
[10] A. Petrovici, K. W. Schmid, and A. Faessler, Nucl. Phys. A **689**, 707 (2001).
[11] K. L. Yurkewicz *et al.*, Phys. Rev. C **70**, 054319 (2004).
[12] K. Yamada *et al.*, Eur. Phys. J. A **25**, 409 (2005).
[13] H. Nann and W. Benenson, Phys. Rev. C **10**, 1880 (1974).
[14] C. J. Chiara *et al.*, Phys. Rev. C **75**, 054305 (2007).
[15] A. P. Zuker, S. M. Lenzi, G. Martinez-Pinedo, and A. Poves, Phys. Rev. Lett. **89**, 142502 (2002).
[16] J. Huo and S. Huo, Nucl. Data Sheets **107**, 1393 (2006).
[17] A. Gadea *et al.*, Phys. Rev. Lett. **97**, 152501 (2006).
[18] D. Rudolph *et al.*, Phys. Rev. C **78**, 021301(R) (2008).
[19] I. Schneider, A. F. Lisetskiy, C. Frießner, R. V. Jolos, N. Pietralla, A. Schmidt, D. Weisshaar, and P. von Brentano, Phys. Rev. C **61**, 044312 (2000).
[20] D. Rudolph, C. Baktash, M. J. Brinkman, M. Devlin, H.-Q. Jin, D. R. LaFosse, L. L. Riedinger, D. G. Sarantites, and C.-H. Yu, Eur. Phys. J. A **4**, 115 (1999).
[21] A. F. Lisetskiy, A. Schmidt, I. Schneider, C. Friessner, N. Pietralla, and P. von Brentano, Phys. Rev. Lett. **89**, 012502 (2002).
[22] C. E. Svensson *et al.*, Phys. Rev. Lett. **82**, 3400 (1999).
[23] D. Rudolph *et al.*, Phys. Rev. Lett. **80**, 3018 (1998).
[24] J. Ekman *et al.*, Phys. Rev. C **66**, 051301(R) (2002).
[25] J. Ekman *et al.*, Phys. Rev. C **70**, 014306 (2004).
[26] R. du Rietz *et al.*, Phys. Rev. C **72**, 014307 (2005).
[27] I.-Y. Lee, Nucl. Phys. A **520**, 641c (1990).
[28] C. E. Svensson *et al.*, Nucl. Instr. Methods A **396**, 228 (1997).
[29] D. G. Sarantites *et al.*, Nucl. Instr. Methods A **381**, 418 (1996).
[30] D. G. Sarantites *et al.*, Nucl. Instr. Methods A **530**, 473 (2004).
[31] A. Gavron, Phys. Rev. C **21**, 230 (1980).
[32] D. Rudolph *et al.*, Phys. Rev. C **63**, 021301(R) (2000).
[33] C. Andreoiu, PhD. thesis, Lund University, 2002.
[34] J. Ekman, PhD. thesis, Lund University, 2004.
[35] D. C. Radford, Nucl. Instr. Methods A **361**, 297 (1995).
[36] J. Theuerkauf, S. Esser, S. Krink, M. Luig, N. Nicolay, O. Stuch, and H. Wolters, program TV, University of Cologne (unpublished).
[37] E. Caurier, shell model code ANTOINE, IReS Strasbourg 1989, 2002; E. Caurier and F. Nowacki, Acta Phys. Pol. **30**, 705 (1999).
[38] E. Caurier and F. Nowacki, Acta Phys. Pol. **30**, 705 (1999).
[39] A. Poves, J. Sanchez-Solano, E. Caurier, and F. Nowacki, Nucl. Phys. A **694**, 157 (2001).

[40] M. Honma, T. Otsuka, B. A. Brown, and T. Mizusaki, Phys. Rev. C **65**, 061301(R) (2002)
[41] M. Honma, T. Otsuka, B. A. Brown, and T. Mizusaki, Phys. Rev. C **69**, 034335 (2004); M. Honma, B. A. Brown, T. Mizusaki, and T. Otsuka, Eur. Phys. J. A **25**, 499 (2005).
[42] E. Caurier, G. Martinez-Pinedo, F. Nowacki, A. Poves, and A. P. Zuker, Rev. Mod. Phys. **77**, 427 (2005).
[43] J. Ekman, C. Fahlander, and D. Rudolph, Mod. Phys. Lett. A **20**, 2977 (2005).
[44] R. du Rietz *et al.*, Phys. Rev. Lett. **93**, 222501 (2004).
[45] E. K. Johansson *et al.*, Phys. Rev. C **77**, 064316 (2008).
[46] D. Rudolph *et al.*, Nucl. Phys. A **694**, 132 (2001).
[47] D. Rudolph, C. Baktash, M. Devlin, D. R. LaFosse, L. L. Riedinger, D. G. Sarantites, and C.-H. Yu, Phys. Rev. Lett. **86**, 1450 (2001).
[48] E. K. Johansson *et al.*, Phys. Rev. C **80**, 014321 (2009).
[49] T. Døssing, S. Frauendorf, and H. Schulz, Nucl. Phys. A **287**, 137 (1977).
[50] D. S. Delion, R. J. Liotta, and R. Wyss, Phys. Rev. C **68**, 054603 (2003).
[51] G. Audi, A. H. Wapstra, and C. Thibault, Nucl. Phys. A **729**, 337 (2003).
[52] H. Junde, Nucl. Data Sheets **87**, 507 (1999).
[53] T. W. Burrows, Nucl. Data Sheets **75**, 1 (1995).
[54] C. E. Svensson *et al.*, Phys. Rev. C **58**, R2621 (1998).
[55] T. Bengtsson and I. Ragnarsson, Nucl. Phys. A **436**, 14 (1985).
[56] A. V. Afanasjev, D. B. Fossan, G. J. Lane, and I. Ragnarsson, Phys. Rep. **322**, 1 (1999).
[57] B. G. Carlsson and I. Ragnarsson, Phys. Rev. C **74**, 011302(R) (2006).
[58] T. Bengtsson, Nucl. Phys. A **496**, 56 (1989).
[59] G. Andersson *et al.*, Nucl. Phys. A **268**, 205 (1976).